

Power Transfer via Metamaterials

C.J. Stevens¹

Abstract: Metamaterials offer new propagation modes for electromagnetic signals which have been explored as media for data exchange. They also offer a good prospect for efficient power transfer. This paper considers the limits on transferable power and their consequences in relation to magneto inductive waves in 1 and 2 dimensional magnetic metamaterial structures. The upper limit is found to be directly related to the voltage tolerance of capacitances used in the meta-material's construction. Higher resonant frequencies offer better efficiency and higher maximum powers. For a proposed device operating in the Qi band (100-200k Hz) power transfer limits of 140 W are derived. The effects of finite length guides on performance and limitations imposed by standing waves and improper termination are explored.

1 Introduction

Metamaterials [Pendry, Holden, Robbins and Stewart (1998)][Pendry, Holden, Robbins and Stewart (1999)] are a subject of continuing study in many areas of science and engineering with a diverse range of potential applications such as super directive antennas, invisibility cloaking systems, medical imaging receivers [Wiltshire, Hajnal, Pendry, Edwards and Stevens (2003)] and more. Recently we considered the use of a magnetic metamaterial [Stevens, Chan, Stamatis and Edwards (2010)] as a medium for near field data transfer and have subsequently showed that such a structure can operate in both one and two dimensions with good data capacity (>300 MB/s) and low noise [Chan and Stevens (2011)]. To date they have not been considered in the field of power transfer although significant work has been devoted to their behaviour as transmission media for high frequency signals and data. This paper deals with the contactless distribution of power to multiple terminals using magnetic, planar, one dimensional metamaterials to form near field coupled magneto-inductive waveguides. These waveguides form a local distributed transmission channel for power transfer to multiple receivers in it's near field.

¹ University of Oxford, Oxford,UK

Wireless power transfer is now a venerable subject with earliest references going back to the 1900s [Tesla (1900)]. More recently the subject has been revived [Liu (2007)] with interest in simplification of wiring and particularly the charging of mobile devices such as laptops and mobile telephones. Long range power transmission using large resonant coils has been the subject of recent research [Kurs, Karalis, Moffatt, Joannopoulos, Fisher and Soljacic (2007)] but alongside this is a developed interest in near field contactless power transfer, particularly for the recharging of batteries in small appliances [Liu (2007)][Neufield (2007)][Kuerschner and Rathge (2008)].

In 2009 the Qi consortium released a standard for small near field wireless power systems based on inductive linkage between source and receiver coils. A variety of transmitter structures are described within this standard with an operating frequency between 110 and 205k Hz [Wageningen and Staring (2010)]. This aims to promote the acceptance and development of wireless battery charging in particular by offering a standard platform for designers to exploit. At present, within this standard, providing power to multiple terminals is provided for using an array of source coils similar to that described in the literature [Liu (2007)] where three layers of coils are enclosed within a 'platform'. These coils are poled to determine which, if any, is in proximity to a receiver and if so the appropriate coil (or coils) are driven to provide power. To achieve this active circuits are required to selectively drive a particular source coil making the complexity of the power transfer surface relatively high.

This work aims to combine the confined but accessible channel of a magneto-inductive waveguide with the concept of a power transfer platform with a view to reducing the complexity of the power transfer structure and enabling simpler, potentially flexible – even wearable devices to be designed.

2 Magneto-Inductive Waves

Many metamaterial structures are composed of arrays of identical coupled resonant electrical circuits – often in the form of magnetically coupled LRC resonators.. An example of such a structure is shown in Figure 1. In 2002 it was shown by Shamonina *et al.* [Shamonina, Kalinin, Ringhofer and Solymar (2002)] that such structures supported a new type of slow wave propagation which has come to be known as Magneto-inductive (MI) waves. Structures that support these waves have come to be known as magneto-inductive waveguides (MIWs).

Referring to Figure 1, excitation of a current in one resonant circuit (cell) of the MIW generates a magnetic flux which in turn may induce a current in the neighbouring cells if their impedance at it's frequency is low enough. In general this

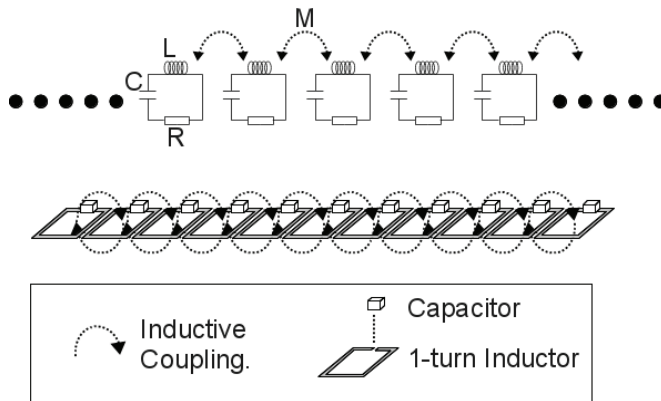


Figure 1: A simple Magneto-inductive waveguide formed from a linear array of inductive loops with series capacitors to form resonating circuits.

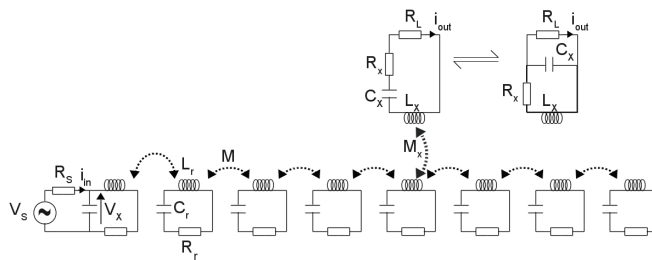


Figure 2: Equivalent circuit for a finite MIP line with a variable location receiver showing to two configurations under consideration for the receiver circuit. The source cell is located at the left hand end of the line with an internal resistance of R_s .

means that signals can propagate along the MIW which are in the vicinity of the resonator's resonance. The potentially strong coupling between cells means that the resonance is spread into a broad band. MI waves occupy this bandwidth controlled by the resonant frequency of, and coupling strength between, cells. The coupling is usually described by the dimensionless parameter K where M_1 is the mutual inductance between nearest neighbour resonators and L_r is the self inductance of each identical resonator in the structure. As the value of K increases the bandwidth for MI wave propagation increases whilst their attenuation decreases. For sufficiently high values of K bandwidths in excess of 50 % have been reported with attenuation as low as 2.3 dB/m [Syms, Solymar, Young and Floume (2010)].

In general power flow in MIW has been derived as the product of the the energy stored in the reactive components and the MIW group velocity [Solymar and Shamonina (2009)]. Here we wish to identify the limits for power transfer and the efficiency with which power may be transferred to a load.

3 MIW Power Transfer Scheme

In our power transfer scheme, as with data [Stevens, Chan, Stamatis and Edwards (2010)] , we wish to be able to place a receiving terminal at any location above the Magneto-Inductive Power Surface (MIP surface) and have it receive power from the source terminal located elsewhere on the device – usually at one end in the case of a one dimensional structure. Critical to this is the need for low loss transmission whilst bandwidth is relatively unimportant. This contrasts strongly with the requirements for data transfer where bandwidth is much more significant in determining overall data rate than loss [Chan and Stevens (2011)]. In fact the key to achieving low loss is strong coupling (high K) between cells in the structure which actually leads to large bandwidth too so both requirements may be met using the same metamaterial configuration.

In general there are two configurations for a purely magnetically coupled structure – axial and planar which correspond to either stacking the resonant circuits along a common axis or placing them in a coplanar configuration with their axes vertical (this is shown in Figure 1). For axial alignment the mutual inductance is positive and may have values up to the maximum possible of $|L_1| = L_r$. In the planar case the mutual coupling is negative and the maximum possible value is much lower than the axial case with the largest ratio reported as $|M_r| = 0.35L_r$ [Solymar and Shamonina (2009)]. For symmetric resonant cells this is even lower with the largest reported at less than $|M_r| = 0.2L_r$.

Figure 2 shows the general MIP scheme wherein a fixed input terminal injects signals into the magneto-inductive waveguide whilst one or more receiving terminals,

located in close proximity to it are able to receive power. In general terminals could have quite different configurations to the cells forming the MIP but in circuit terms this only changes their LRC values and the coupling they achieve with the cells of the waveguide via M_x . Power is injected at the first cell of the MIP in this scheme and is available at any point on the structure. For a finite line reflections from the far end of the structure will generate standing waves that may prevent some receiver locations from obtaining efficient power transfer unless the source is able to adjust its operating frequency to shift the standing wave nodes away from active terminals.

4 Limits to magneto-inductive power transfer

In order to optimise the performance of the device it is necessary to explore its limits from a theoretical standpoint. Power is transferred along the MIP surface by currents circulating in each cell. As the power flowing increases so does the magnitude of the current in each cell. In general one may assume that the resistance associated with the PCB tracks forming each inductor is low (typically $R_r < 100m\Omega$ for a 40mm square formed from PCB tracks 1mm wide and $25\mu m$ thick for frequencies < 250 MHz). In this case the main factors limiting the power transferred are the breakdown voltage of the resonator capacitors which constrains the maximum current that can circulate in any cell and the attenuation of magneto-inductive waves as they propagate to the receiver.

In order to evaluate the maximum possible power delivered it is useful to consider the matching condition for MIWs which is that the load impedance [Syms, Solymar and Shamonina (2005)] in a receiving terminal should have the value of

$$Z_T = j\omega M_1 e^{-\gamma d} \quad (1)$$

In order to match the magneto-inductive wave and produce no reflection of signal back to the source. Here d is the spatial period of the structure, M_1 is the nearest neighbour mutual inductance and γ is the complex propagation constant derived from the MIW dispersion equation by

$$\cosh(\gamma d) = \frac{-Z_r}{2j\omega M_1} \rightarrow \gamma d = \cosh^{-1} \left(\frac{R_r + j(\omega L_r - 1/\omega C_r)}{-2j\omega M_1} \right) \quad (2)$$

and R_r is the resistance of each cell, M_1 is the first order mutual inductance between nearest neighbouring cells and C_r is the series capacitance in each cell. The terminating impedance Z_T is complex and very hard to match for broadband signals but in the case of power we require only a single frequency to excite. If one chooses the resonant frequency of the MIW cells $\omega_0 = 1/\sqrt{L_r C_r}$, then Z_T becomes pure

real and may be evaluated using the standard logarithmic form for inverse cosh ($\cosh^{-1}(z) = \ln(z + \sqrt{z+1}\sqrt{z-1})$) with a value that is given by equation 3.

$$Z_T(\omega_0) = \frac{2\omega_0^2 M_1^2}{R_r + \sqrt{R_r^2 + 4\omega_0^2 M_1^2}} \quad (3)$$

where the positive root is chosen to ensure a positive real value for Z_T . For very low loss lines where $R_r \rightarrow 0$ the resonant termination impedance $Z_T(\omega_0) \rightarrow \omega_0 M_1$.

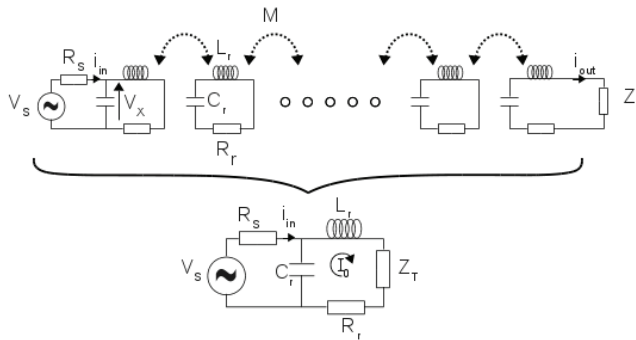


Figure 3: Equivalent circuits for power transfer calculation. Z_T models the infinite line or a perfectly matched load. Upper – input terminal and line with a terminating load, Lower – equivalent circuit exploiting the matched load to model the entire infinite line.

Proceeding to evaluate the power delivered we assume a configuration whose equivalent circuit is shown in Figure 3.

Here output is modelled under the assumption that the receiver placed on the N^{th} resonator in the 1D line is equivalent to inserting a matched load into that resonator of value Z_T . Before proceeding to compute the output power it is important to consider where in the system the capacitors are exposed to the greatest potential. For the simple 1D line of Figure 3 the maximum circulating current is at the first cell I_0 so it is here that the limitation on breakdown voltage is most significant. To determine the maximum input power that can be injected we refer to the lower circuit of Figure 3 in which the semi-infinite MIW is described by a single matching impedance Z_T . The input power transferred into the MIW is then:

$$P_{IN} = |I_0|^2 \mathcal{R}(Z_T) \quad (4)$$

Where $\mathcal{R}(Z_T)$ is the real part of the matching impedance. The power delivered to a matched load at the end of a line of N cells is then given by the amplitude of the current circulating in the receiving resonator I_R which is the current in the N^{th} cell, using

$$P_{OUT} = |I_0 e^{\gamma Nd}|^2 \mathcal{R}(Z_T) \quad (5)$$

Where N is the number of cells between the source and the receiver whilst the input power is given by the same expression but with $n = 1$. The propagation constant $\gamma = \alpha + j\beta$, where α is the attenuation and β the phase constant. Hence the maximum power that can be injected to an MIW, at the resonant frequency is

$$P_{IN} = |I_0^{max}|^2 \frac{2\omega_0^2 M_1^2}{R_r + \sqrt{R_r^2 + 4\omega_0^2 M_1^2}} \approx |I_0^{max}|^2 \frac{2R_r \omega_0^2 M_1^2}{1 + 2\omega_0 M_1 / R_r} \quad (6)$$

where $e^{-j\beta Nd} = 1$ and the approximation is made for a relatively strongly coupled line in which $R_r \ll \omega_0 M_1$. Now, knowing the input current in the first element of the line we can compute the maximum possible output power from the system. Equation 2 holds true for this case as well and the maximum power is then limited by the potential applied across the capacitor at the input terminal being less than V_B . In this case the maximum circulating current I_0^{max} is given by

$$I_0^{max} = \frac{V_B}{j\omega_0 L_r + R_r + Z_T} \quad (7)$$

and the maximum input power then calculated by combining equations 6 and 7.

$$\frac{P_{IN}}{V_B^2} = \frac{Z_T(\omega_0)}{[R_r + Z_T(\omega_0)]^2 + \omega_0^2 L_r^2} \quad (8)$$

In order to derive the maximum output power possible at resonance one then multiplies this by the transmission $e^{-2\alpha Nd}$ with the attenuation constant determined using the real part of γd from equation 2.

$$\frac{P_{OUT}}{V_B^2} = \frac{Z_T(\omega_0) e^{-2\alpha(\omega_0)Nd}}{[R_r + Z_T(\omega_0)]^2 + \omega_0^2 L_r^2} \quad (9)$$

Which enables the maximum limit for power transfer at resonance to a load to be determined. In order to illustrate the behaviour described by equations 7 & 8 Figure 4 shows the values for maximum possible P_{IN}/V_B^2 and P_{OUT}/V_B^2 with $k = 0.4$, $L = 138$ nH and $R = 0.1 \Omega$. These values match well with real structures such as that

shown in Figure 3 with cell periods on the order of 40 mm. The length of the structure is varied from 1 cell to 16 cells (the input cell is not considered part of the line here so $N = 1$ is two cells long). The resonator capacitance C_r is varied in each case according to the required resonant frequency. There is a clear peak in the maximum possible output power with one frequency being superior for each given length. This peak power frequency shifts to higher values with increasing device length and the peak power drops at the same time.

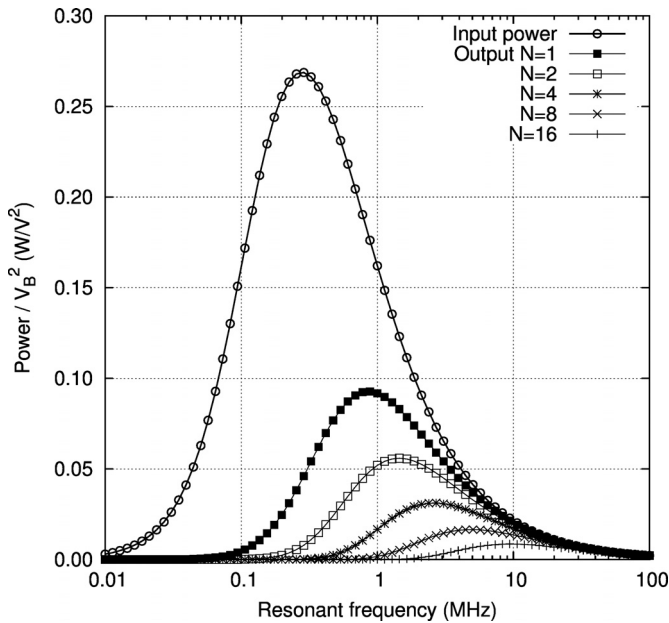


Figure 4: Resonant Input and output powers for MIW structures of various lengths terminated by a perfect matching impedance as a function of the cell's resonant frequency.

This behaviour can be understood as the consequence of two effects. Firstly the magnitude of the current circulating in the input cell I_0 falls at -10 dB/decade for frequencies above $\omega_0 = R_r/M_1$ whilst the matching impedance rises at +10 dB/decade above this point which means that there is a peak in P_{IN}/V_B^2 . Simultaneously the attenuation at resonance falls with increasing frequency so that the transfer function $e^{-2\alpha Nd}$ is very small for low frequencies rising at +20 dB/decade until it reaches unity for high frequencies. The rising transfer function shifts the peak of P_{OUT}/V_B^2 to higher frequencies as the number of cells and hence the overall attenuation increases.

It would seem from these results that efficiency should be very low however the ratio P_{OUT}/P_{IN} is only the magnitude of the transfer function $e^{-2\alpha Nd}$ which tends to unity at high frequencies as is nearly inversely proportional to ω_0 (for fixed R_r). Hence the efficiency is higher at high resonant frequencies whilst the maximum possible power is lower making any attempt to design a power transfer system a balance between these two parameters along with a consideration of the expected length of the structure.

5 Component limitations

In order to maximise the power that can possibly be transferred to a load we need as low a cell resistance (R_r) as possible to obtain a low attenuation, a resonant frequency that matches the peak of P_{OUT} and as high a capacitor breakdown voltage as possible. Ultimately the breakdown of the capacitor in the input cell is the limiting feature with attenuation then restricting the power available. This is problematic – the major breakdown mechanism in most capacitors relates to their dielectric breakdown field E_{br} and hence the maximum potential they can sustain (V_B) is proportional to the inverse of capacitance for any particular dielectric (permittivity ϵ_r). Taking the thin parallel plate capacitor as a simple example with plate area A this relationship is:

$$V_B = \frac{A\epsilon_0\epsilon_r E_{br}}{C} \quad (10)$$

Whereupon attempting to achieve too low a resonant frequency, requiring too large a capacitance results in a serious reduction of the limit on V_B and hence the maximum power. In general manufacturers of capacitors do not specify the dielectric breakdown field but rather a fixed maximum breakdown voltage in which case one may consider the breakdown voltage to be a constant for any given capacitor series. For small surface mount multilayer ceramic capacitors, the breakdown voltage relates to the spacing between plates in the stack of layers from which the device is formed whilst the capacitance is varied by adjusting the number of layers used (effectively changing A). Figure 5 shows typical ranges taken from a catalogue of components available in 2012 (Kemet Ltd 2012). There is a clear boundary formed by the maximum values of C and V_B here which is approximately $C_{max} \propto V_B^2$ suggesting that edge effects or other design factors like surface roughness are having a significant effect at high voltages or capacities.

Taking these values for V_B and C_{max} one may compute the optimum operating frequencies and maximum powers for a simple device using equation 9. In this case the capacitance for the resonant cells is taken as the constant and the cell inductance varied in order to adjust the cell's resonant frequency. Figure 6 shows the computed

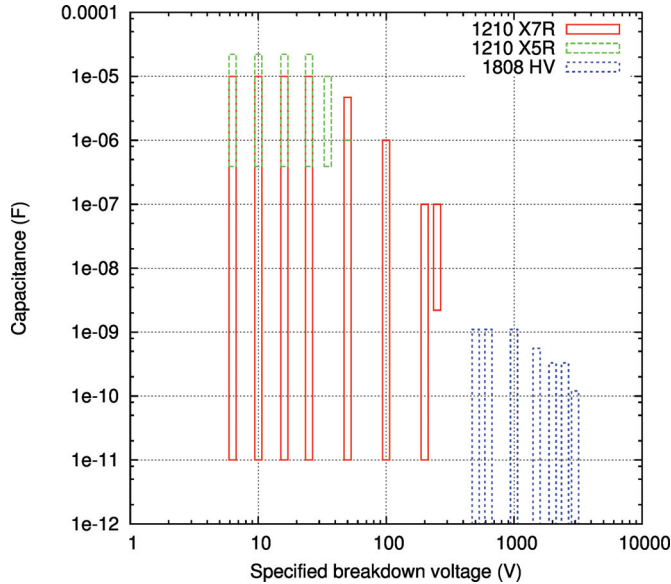


Figure 5: Range of values for various surface mount capacitors versus specified breakdown voltage (Kemet Catalogue 2012)

maximum power outputs for a 10 cell line using the highest value capacitors from each series shown in Figure 5 with the cell resistance set to 0.1Ω and a coupling strength of $K = 0.4$. Indicated on the Figure are some of the ISM frequency bands plus the frequency range used by the proposed wireless power standard known as Qi [Wageningen and Staring (2010)]. Figure 5 implies a strong correlation between low capacitance and high breakdown voltage. In Figure 6 the maximum power limit increases dramatically with rising V_B whilst the optimum frequency also rises with decreasing capacitance. The maximum power is in fact independent of the capacitance – this only controls the optimum frequency whilst the optimum power is only dependent on the breakdown voltage. Higher capacitance lowers the optimum frequency but generally suffers from a lower breakdown voltage and hence a lower power capability.

These results may seem in opposition to those shown in Figure 4 but the strong increase in breakdown voltage for lower capacitance values means that not only is the attenuation decreasing as the effective Q factor of cells rises but so is the maximum allowed input signal.

Considering the potential applications for this kind of contactless technology, the recharging of small batteries as used in mobile personal electronics (such as tele-

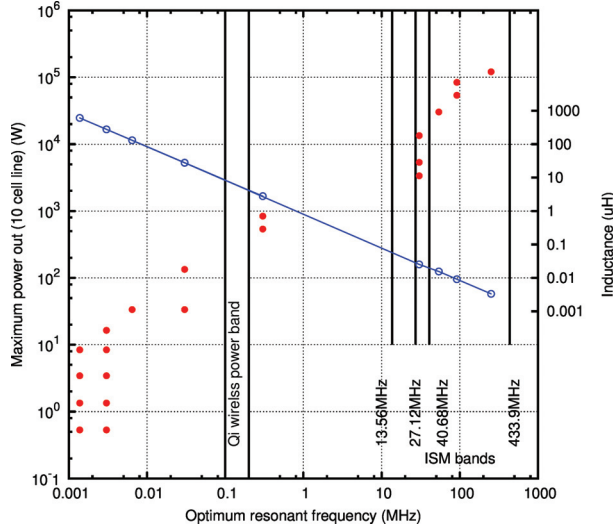


Figure 6: Maximum output power against optimal frequency for the capacitors shown in Figure 5. The inductance required for each optimum frequency is also shown.

phones and media players) requires only ~ 10 W or less and would hence be possible using frequencies from a few kHz upwards. For frequencies within the Qi band (100 - 205 kHz) the maximum power transfer possible for these ceramic capacitor loaded structures would be in excess of 100 W (using 300 nF capacitors with $V_B = 100$ V). At higher frequencies – for instance the 13.56 MHz ISM RF power bands maximum power levels increase dramatically to over 800W (in the main because $V_B = 250$ V for optimal frequencies in this range).

Over the range of capacitances considered in Figure 6 the inductance required for optimal resonant frequency is widely varying. For the Qi band inductances of between 4.2 and 8.3 μH are required, rather higher than simple single turn structures can easily meet, but achievable with multi-turn coils. In this case the challenge is to raise the inductance with extra turns whilst maintaining the required value of K.

6 Finite Structures

The preceding discussion has been based on a perfectly terminated MIW with the power absorbing load being perfectly matched to the structure at its end. The more realistic situation we would like to consider is however a finite length of magneto-inductive waveguide where a receiving terminal is placed in proximity to one of its cells at any point on the structure. In this case the coupling of the receiving terminal

to the device is likely to become important in both facilitating power transfer and limiting the efficiency at which power may be delivered.

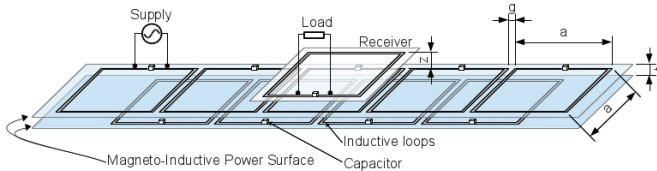


Figure 7: Magneto-Inductive Power Surface formed from two overlapping Magneto-Inductive Waveguides with a power receiver positioned above one cell.

Figure 7 shows our proposed structure for power transmission where the MIP surface is formed using two magneto-inductive waveguides placed on top of one another with the lower line shifted half a period from the upper. This structure is admittedly more complex than the general scheme shown in Figure 2 with second and third order mutual inductance being now significant contributors to the overall coupling. Our previous work [Radkovskaya, Sydoruk, Shamonin, Stevens, Faulkner, Edwards, Shamonina and Solymar (2007)] has shown that this configuration gives a strong coupling between cells and hence offers a very low loss, wideband channel although second and third order coupling tends to be more significant in this device and cannot be ignored.

In the shifted design the cells of the MIWs are formed using square single turn inductive loops fabricated as tracks on two sides of a substrate using surface mount capacitors to form LRC resonant circuits. The AC power supply is connected directly across the capacitor in the first cell at one end of the structure whilst the receiver is located above the MIP surface at a height of z above the top layer. The power receiver is also formed using an identical resonator to those forming the surface with the load connected in parallel with its resonator capacitance.

Our design assumes that we intend to provide power to charge one or more small portable devices and so the scale of the structure assumes that the receiver must fit into the footprint of their enclosures. We assume therefore that the cell period is $10 \text{ mm} < d < 40 \text{ mm}$ and that the gap between inductors $g = 0.5 \text{ mm}$. Top and bottom layers of the MIP are assumed to be fabricated on a typical printed circuit board stock with a thickness of $t = 1.6 \text{ mm}$. As a design constraint we have selected the resonant frequency of the cells to be at one of the ISM bands (13.56 MHz) often used as RF power signals in plasma processing amongst others. In general any frequency may be chosen for the system although much lower frequencies require larger LC products to resonate most likely requiring multi-turn inductors and bigger

capacitance for frequencies below 1 MHz.

As an example consider the largest size cells with a period of 40mm whose side lengths are 39.5 mm with tracks 1 mm wide. The equivalent circuit parameters for this configuration are given in table 1.

Table 1: Equivalent circuit parameters for finite line calculations. K is the dimensionless coupling ratio $k = 2M/L$

L=138 nH	$M_1=25.9$ nH (K=0.37)
R=78 m Ω	$M_2=-14.8$ nH (K=-0.21)
$M_x=37.9$ nH (K _x =0.55)	$M_3=-1.53$ nH (K=-0.02)

For a finite length of waveguide without a matched load terminating its endpoint there will be strong reflection of power back along the guide towards the source resulting in standing waves being formed. In the worst case standing waves may double the voltage applied to the capacitors in cells located at their antinodes resulting in a drop by a factor of 4 in the maximum power that may be transferred for a particular capacitor breakdown potential. With a receiving terminal coupled to the waveguide the exact behaviour of standing wave modes is sensitive to the degree of matching that the receiver achieves with the guide. Strongly coupled terminals should absorb a significant portion of the available power resulting in very small standing wave amplitudes and allowing the maximum power to approach that for the perfectly terminated case described by Figure 6.

Using the parameters from table 1 one may compute the power ratio P/V^2 for this line and the result is shown in Figure 8 for which the maximum occurs at a resonant frequency of 5.6 MHz with a peak value of $1.35 \times 10^{-2} \text{W/V}^2$. Two frequencies either side of this peak were chosen to investigate using the numerical simulation of the finite line and these are indicated on Figure 8. One is close to the peak and the other at the 13.6 MHz ISM frequency.

In order to evaluate the limits for the finite line with near field coupled receiving terminals we must resort to discrete circuit simulation techniques in which the combined system of magneto-inductive waveguide and receiver is modelled using equivalent circuits via the impedance matrix [Stevens, Chan, Stamatis and Edwards (2010)]. Our model proceeds based on the equivalent circuits of Figure 2 with second and third order coupling included.

The line is still excited using a source of internal resistance R_s directly driving the first cell in the line but now the receiver is coupled via a variable mutual inductance M_x to any of the cells in the finite line. M_x must be considered variable as it's value

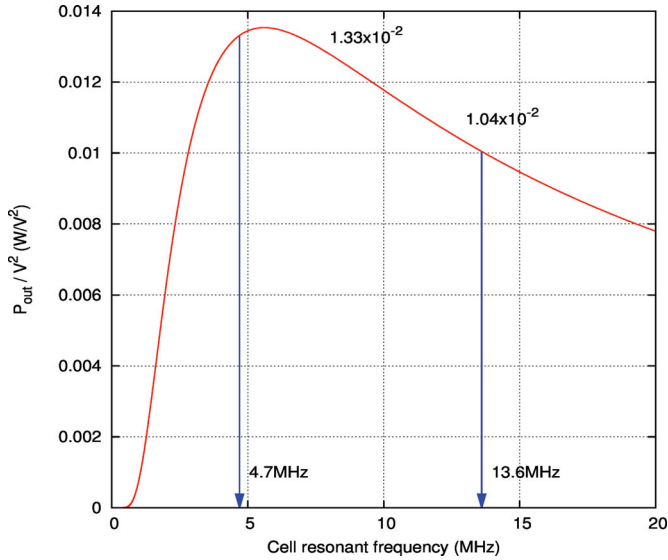


Figure 8: Predicted power transfer end to end for 40mm cell period showing the two cases considered in the finite model.

can significantly affect the overall efficiency of the system and is dependent on the height at which the receiver is located above the line. The exact configuration of the receiver's load can be either as series connected or as parallel connected load resistance

In order to explore the behaviour of this system here we concentrate on a line containing 11 cells (including the source cell) with the receiver positioned above any of the cells. Using a 12x12 impedance matrix we are able to determine the current in each cell and the receiver as a function of the driving frequency f , load resistance R_L and coupling inductance M_x . For each cell we solve

$$V_n = I_n Z_n + j\omega M_1(I_{n+1} + i_{n-1}) + j\omega M_2(I_{n+2} + i_{n-2}) + j\omega M_3(I_{n+3} + i_{n-3}) \quad (11)$$

Where $V_n = 0$ for all $n > 1$. V_1 is the source voltage amplitude and this is set at the breakdown limit for the resonator capacitors (250 V in this case) in order to obtain a comparable value to the predictions shown in Figure 6.

Figure 9 shows the results for two resonant frequencies of 4.7 and 13.6 MHz simulated by using 1 nF and 8.3 nF resonating capacitors respectively. Both these values are available with breakdown voltages of 250 V and so this value was chosen for the input signal level. In fact 1 nF is available up to a breakdown of 1000 V which would allow a 16 times greater maximum power for the 13.6 MHz case. In both

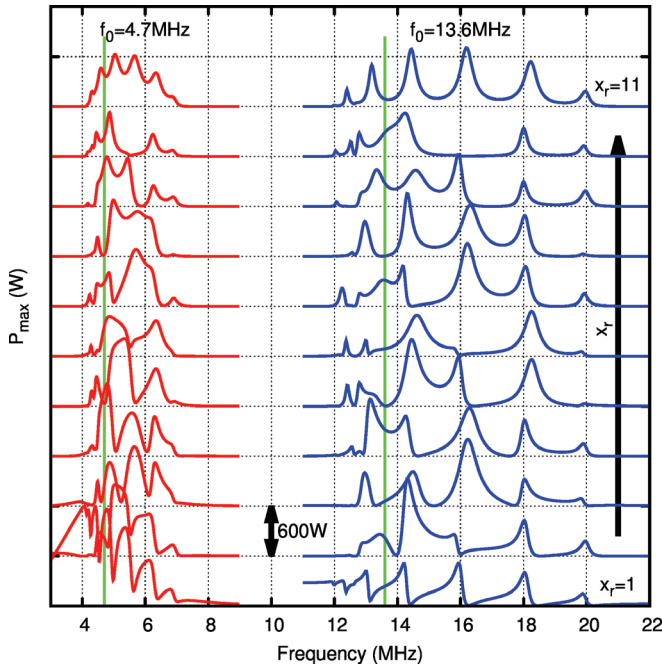


Figure 9: Output powers for two 10 cell MIPs formed from 39.5 mm square cells with differing tuning capacitors to adjust their resonant frequencies. Powers are calculated for $250 V_{peak}$ at the source which is achievable for these resonant frequencies. Dotted lines indicate the resonant frequencies of the MWP cells in each case.

cases a clear passband with strong transmission is present. For these calculation the receiving terminal was assumed to be located 1.6mm above the top waveguide layer (modelling the thickness of a PCB on which it may be built).

The large bandwidth of the shifted waveguide structure is clear with both having a fractional bandwidth ($\Delta f/f_0 \approx 0.6$) The higher frequency device exhibits very clearly spaced resonant peaks within its passband whilst the lower frequency device generates more closely spaced peaks with a smoother passband for most locations. As the receiving terminal location is scanned along the length of the device there is clearly a variation in the power received as a function of frequency along with a variation in the frequency for which power transfer is optimal.

Figure 10 collates the peak powers and frequencies for the two examples. The powers transferred in both cases to the receiver are quite similar for all locations except where there is direct coupling between the source and the receiver ($n = 1$).

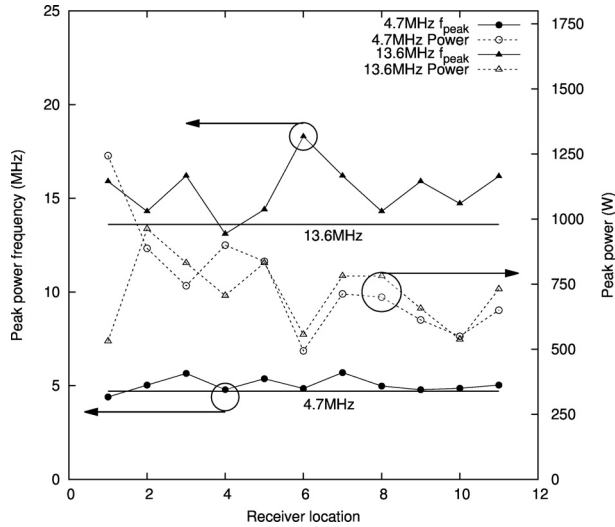


Figure 10: Peak powers transferred and optimum frequencies for the two MWP lines simulated.

A general decay in power transferred is clear with the modulation arising from standing waves still evident. The symmetrical centre of the line is clearly a bad location for a receiver as a large number of standing wave modes contribute here. In practice it may be better to use this symmetry point as the source location for the system to reduce the attenuation between source and receivers.

In both cases the best power for each location is nearly always available at a frequency **higher** than the cells resonant frequency suggesting that the maximum possible power derived using equation 9 (based on the power being transmitted at the resonant frequency) may not be the final limit with the generalised optimal case being a frequency somewhat above this.

7 Conclusions

This paper has begun the development of contactless power transfer technology based on magneto-inductive waves. In general for power one might expect lower frequencies to be preferred but this work has found that the limits imposed on circulating current by capacitor breakdown result in much better performance at higher operation frequencies. Magnetoinductive wave attenuation further limits the low frequency performance with losses increasing inversely to resonant frequency. The strength of coupling between resonators strongly affects the overall maximum power transferable and large couplings are preferred. Some difficulty may be ex-

pected however in coupling receivers efficiently to magneto-inductive waveguides with very strong coupling.

The efficiency for power transfer increases dramatically with the optimum resonant frequency but for the structures analysed here was only 50 % at 4.7 MHz and 70 % at 13.6 MHz. For very efficient power transfer much higher resonant frequencies will be required. High frequency also favours the increase of the maximum possible transfer as smaller capacitances generally have higher breakdown voltages. For the 431 MHz ISM band power transfer in excess of 120 kW is possible using ceramic capacitances.

Design of an MWP to meet the Qi standard [Wageningen and Staring (2010)] is possible with a power limit of 140 W imposed by the ceramic capacitors limits. To achieve this would require resonant cells with inductances of 4 μH or higher. Achieving this in a small footprint compatible with typical mobile electronics footprints is possible but would most likely require multi-layer PCB coils with 4 - 8 turns and track widths of ~ 0.1 mm..

Future applications for this technology may include the development of wireless integrated circuit packages which are powered by MWP structures which also provide for data exchange. For power transfer between IC packages on this type of wireless integrated circuit high power and efficiency arising from a high choice of operating frequency would be most beneficial for both efficient power transfer and high bus speeds.

We would like to acknowledge the support of Oxford University and ISIS innovation Ltd in the preparation of this paper.

References

Chan C.W.T., Stevens C.J. (2011): Two-dimensional magneto-inductive wave data structures. *Proceedings of the 5th European Conference on Antennas and Propagation (EUCAP)*, pp.1071-1075.

Kuerschner D, Rathge C. (2008): Contactless energy transmission systems with improved coil positioning flexibility for high power applications. *Proceedings of the 39th Power Electronic Specialists Conference (PESC)*, pp.4326.

Kurs A., Karalis A., Moffatt R., Joannopoulos J., Fisher P., Soljacic M. (2007): Wireless power transfer via strongly coupled magnetic resonances. *Science* 317, pp.83-86.

Liu X. (2007): Equivalent Circuit Modeling of a Multilayer Planar Winding Array Structure for Use in a Universal Contactless Battery Charging Platform. *IEEE Transactions on Power Electronics* 22, 1, pp.21-29.

- Neufield R.** (2007): Contactless energy transfer: mobile power on the go. *Plant Engineering* 61, pp.21-22.
- Pendry J., Holden A., Robbins D., Stewart W.** (1998): Low frequency plasmons in thin-wire structures. *Journal of Physics-Condensed Matter* 10, pp.4785-4809.
- Pendry J., Holden A., Robbins D., Stewart W.** (1999): Magnetism from conductors and enhanced nonlinear phenomena. *IEE Transactions on Microwave Theory and Techniques* 47, pp.2075-2084.
- Radkovskaya A., Sydoruk O., Shamonin M., Stevens C., Faulkner G., Edwards D., Shamonina E., Solymar L.** (2007): Transmission properties of two shifted magnetoinductive waveguides. *Microwave and Optical Technology Letters* 49, pp.1054-1058.
- Shamonina E., Kalinin V., Ringhofer K., Solymar L.** (2002): Short dipole as a receiver: effective aperture shapes and streamlines of the Poynting vector. *IEE Proceedings-Microwaves Antennas and Propagation* 149, pp.153-159.
- Solymar L., Shamonina E.** (2009): *Waves in Metamaterials*. Oxford University Press.
- Syms R., Solymar L., Young I., Floume T.** (2010): Thin-film magneto-inductive cables. *Journal of Physics D: Applied Physics* 43, pp.055102.
- Syms R., Solymar L., Shamonina E.** (2005): Absorbing terminations for magneto-inductive waveguides. *IEE Proceedings-Microwaves Antennas and Propagation* 152, pp.77-81.
- Stevens C.J., Chan C.W.T., Stamatis K., Edwards D.J.** (2010): Magnetic Metamaterials as 1-D Data Transfer Channels: An Application for Magneto-Inductive Waves. *IEE Transactions on Microwave Theory and Techniques* 58, pp.1248-1256.
- Tesla N.** (1900): *Apparatus for Transmission of Electrical Energy*. US Patent #649621.
- Wageningen D, Staring T.** (2010): *The Qi Wireless Power Standard*. 14th International Power Electronics and Motion Conference S15, pp.25-32.
- Wiltshire M., Hajnal J., Pendry J., Edwards D., Stevens C.** (2003): Metamaterial endoscope for magnetic field transfer: near field imaging with magnetic wires. *Optics Express* 11, pp.709-715.